Short communication

The Calcined Soils Can Be Used as Anode Materials for Lithium Ion Batteries

Keqiang Ding[1,3], Xiaomi Shi[1], Hui Wang [3], Chenxue Li[1], Wang Wang[1], Hongmin Dou[3], Xiaojing Gao[1], Jingwei Han[1], Junqing Pan[2*]*

[1] College of Chemistry and Materials Science, Hebei Normal University, Shijiazhuang, Hebei, 050024, P.R. China
[2] State Key Laboratory of Chemical Resource Engineering, Beijing University of Chemical Technology, Beijing, 100029, P.R.China
[3] Hebei LingDian New Energy Technology Co., Ltd, Tangshan, Hebei, 064200, P.R.China
[*]E-mail: dkeqiang@263.net

An interesting finding, that the calcined soils can be used as the anode materials for lithium ion batteries (LIBs), is issued for the first time in this work. In the present work, the soils were respectively sintered at $200\,℃$, $400\,℃$, $600\,℃$ and $800\,℃$ for 2 h, leading to the formation of material a, b, c and d. All the prepared materials were carefully characterized by XRD which indicated that SiO_2 was the main component in all resultant materials. SEM images strongly indicated that the morphologies of the resultant materials were closely related to the calcination temperature, and when the calcination temperature was increased from $200\,℃$ to $800\,℃$, the lumpy particles were converted into plate-like particles. The consequences of the electrochemical measurements documented that all the prepared materials could deliver a discharge capacity. Interestingly, the discharge capacity of material c was maintained at about 30 mAh g^{-1} under the current density of 100 mA g^{-1} after 20 cycles. Although the discharge capacity reported in this work was lower when compared to the currently reported anode materials, this interesting finding was very meaningful to the development of anode materials, owing to the abundant resources of soil and the rather lower preparation cost as well as the very simple preparation process.

1. INTRODUCTION

The main objective of this work is to show the interesting finding that the calcined soils can be utilized as anode materials for LIBs.

Generally, a lithium-ion battery mainly consisted of anode, cathode, electrolyte and separator, and the electrochemical performances of an LIB were primarily determined by the properties of the anode and cathode materials [1]. Of late, besides the research works regarding cathode materials, the research work concerning anode materials has also been paid much more attention chiefly because of the following issues [2]. (1) The relatively lower theoretical capacity (372 mAh g^{-1}) of graphite. It is well known that graphite as anode material has been commercialized in LIBs for many years due to its lower cost and satisfied cycling stability. In recent years, the emergence of haze weather in some Asian regions stimulates the development of electric vehicle, as a result, the production of LIBs with higher power densities becomes urgent and significant. Increasing the capacity of anode material is a feasible way to promote the power density of a LIB since the power value is the product of current and voltage [3]. (2) The safety issue of LIBs using graphite as the anode material. Due to the fact that the electrode potential of graphite is close to that of metallic lithium, thus, Li dendrites will form on the surface of graphite especially when being overcharged, which may further produce safety issue like short circuit and fire accidents under some special conditions [4]. (3) The formation of solid electrolyte interphase (SEI) layer on the surface of graphite. It has been reported that a kind of SEI layer, which was generally resulted from the reduction reaction of the electrolyte, would appear on the surface of graphite during use, and the formed SEI layer was disadvantageous to the electrochemical performance of a lithium ion battery [5]. Thus, seeking for a novel kind of anode material to replace graphite becomes an important task for the LIBs-related researchers.

To our knowledge, novel kinds of carbon, transition metal oxides, elementary substance and lithium ions-contained metal oxides are thought as the main four kinds of newly developed anode materials. New kinds of carbon chiefly referred to graphene [6], carbon nanotubes [7], carbon nanofiber [8] and carbon nanodots [9]. Transition metal oxides generally contained Fe_3O_4 [10], Fe_2O_3[11], SnO_2 [12], Co_3O_4 [13] and NiO [14]. And Si [15] and Sn [16] are the main two kinds of elementary substances developed recently. Lithium ions-contained metal oxide mainly included lithium titanate ($Li_4Ti_5O_{12}$) [17] and M_2O_4-based materials [18]. Although, as mentioned above, many novel kinds of anode materials have been developed recently, the practical applications of those newly produced anode materials in the commercial LIBs are very limited, which was mainly caused by the relatively higher preparation cost and the poor electrochemical performance. As far as we know, the usage of the rare metals and the complicated preparation process are the main two reasons which can result in a higher preparation cost of LIBs. The poor electrical conductivity of the anode material and the huge volume variation of the anode material in cycling are the other two reasons which are closely related to the poor electrochemical performance of a LIB. Therefore, developing novel kind of anode materials for LIBs is still a pressing task in the LIBs research field. To the best of our knowledge, no paper reporting the utilization of calcined soil as the anode material of LIBs was published so far.

In this work, anode materials were synthesized directly by sintering the soils at different temperatures. The soils calcined at 200 °C, 400°C , 600°C and 800 °C were denoted as material a, b, c and d, respectively. The electrochemical measurement results indicated that all the prepared materials were able to deliver a discharge capacity though the discharge capacity values were lower as compared to that of the currently reported anode materials, and amongst the prepared materials, material c showed the best electrochemical performance, namely, the discharge capacity value of material c was
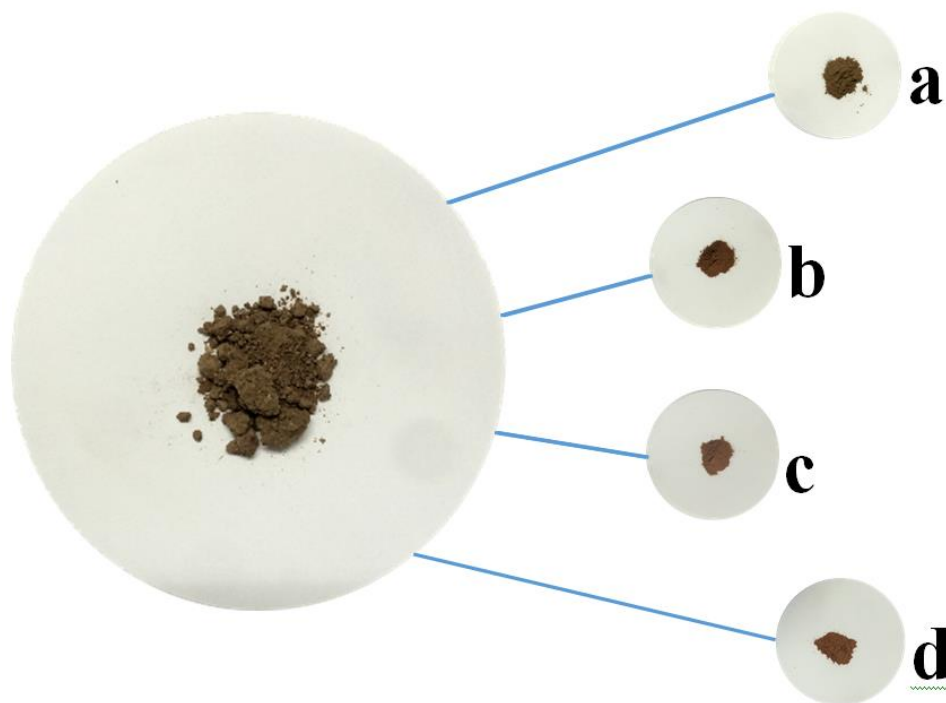
about 30 mAh g^{-1} after 20 cycles at the current density of 100 mA g^{-1}. Although the electrochemical performance of the calcined soils was poor when compared to other kinds of anode materials, a novel group of anode materials was really found in this paper. This work was very beneficial to the development of anode material of LIBs mainly thanks to the abundant resources and the extremely simple preparation process.

2. EXPERIMENTAL

2.1. Materials

Soils were directly gathered from North China Plain. All other chemicals were bought from Tianjin Chemical Reagent Co. Ltd. All materials used in the battery property measurement, such as polyvinylidene fluoride, acetylene black, 1 M LiPF$_6$ electrolyte and the cells, were purchased from Tianjin Lianghuo S&T Developing Co. Ltd. All the chemicals were used as-received and no further purifications were conducted.

2.2. Preparation of the calcined soil anode materials

Scheme 1. Photos for all the produced materials.

Briefly, the gathered soil was dried first in an air dry oven at 80 °C for 2 h, and then, the well dried soil was ground in an agate mortar for about 30 min to create the dried soil powders. Subsequently, the produced powders were pressed into pieces using a manual tablet machine. At last, the resultant pieces were, under the air conditions, sintered in a muffle furnace at different

temperatures, and all the calcination periods were kept identical to be 2 h. After the calcination process, the muffle furnace was cooled down to the room temperature naturally. Again, after a thorough grinding, the final products were prepared. The soils calcined at 200 °C, 400 °C, 600 °C and 800 °C were called as material a, b, c and d, respectively. The photos for the synthesized materials are shown in Scheme 1. Two conclusions can be drawn after a careful observation of these photos. (1) It seemed that the particle sizes of soils became smaller after the calcination treatment. (2) The color of the soils was altered from dark brown to light yellow when the calcination temperature was increased from 200°C to 800 °C. It indicated that the composition of resultant samples varied correspondingly, which probably could influence the electrochemical performance of the synthesized materials.

2.3. Characterization

The composition and the crystal structure of the obtained materials were studied by using X-ray diffraction (Bruker AXS, D8 ADVANCE (Database version PDF-2004), Germany). The morphologies of the resultant materials were examined by scanning electron microscopy (HITACHI, SEM S-570). The elemental composition of the as-prepared materials was studied by using Energy dispersive spectrometer (EDS, INCA Energy 350, England). Fourier transform infrared spectrometry (FT-IR, Hitachi FT-IR-8900 spectrometer, Japan) was employed to detect the functional groups in the samples.

The electrochemical testing techniques, such as cyclic voltammetry (CV) and electrochemical impedance spectroscopy (EIS), were all carried out on a personal computer-controlled CHI 660B electrochemical workstation (Shanghai Chenhua Apparatus, China). In the EIS measurements, the amplitude of the alternating current (AC) was 5 mV, along with a frequency range of 100 kHz-0.1 Hz. All the experiments were accomplished at room temperature.

The battery properties of the prepared materials were measured by using a two-electrode cell, which mainly contained a working electrode and a counter electrode. The counter electrode was a lithium slice. And the working electrodes coated with the materials were fabricated basing on the following process. Firstly, the prepared materials, acetylene black and polyvinylidene fluoride were, at a weight ratio of 8:1:1, thoroughly mixed together to form a mixture. And subsequently, the resultant mixture was stirred vigorously after the addition of several drops of N-methyl pyrrolidone (NMP) which finally led to the formation of slurries. After that, the obtained slurries were carefully painted on a copper foil using a glass piece, and lastly, the Cu piece coated with the slurries was dried in a vacuum drying oven at 120 °C for 6 h to generate the final working electrode. Approximately, the loading of a working electrode was about 1.5 mg cm^{-2}. Besides the working electrode and counter electrode, the two-electrode cells, i.e., the half-cells, also consisted of an electrolyte of 1 M LiPF$_6$ and Celgard 2400 separator, which were constructed in a high pure nitrogen-filled glove box (ZKX type of Nanjing NANDA instrument factory). Also, the solvent of the 1 M LiPF$_6$ electrolyte was a mixed solvent which contained dimethyl carbonate (DMC), ethylene carbonate (EC), ethyl methyl carbonate (EMC) and vinylene carbonate (VC). In this measurement, the metallic lithium foils were used as both the reference and auxiliary electrodes. The electrodes assembled by material a, b, c and d were nominated as electrode a, b, c and d, respectively. The battery property measurements were

accomplished on an apparatus of CT-3008W-5V20mA-S4 (Shenzhen Neware Electronics Co., Ltd. China). The charge and discharge potential range was from 0.01V to 3 V.

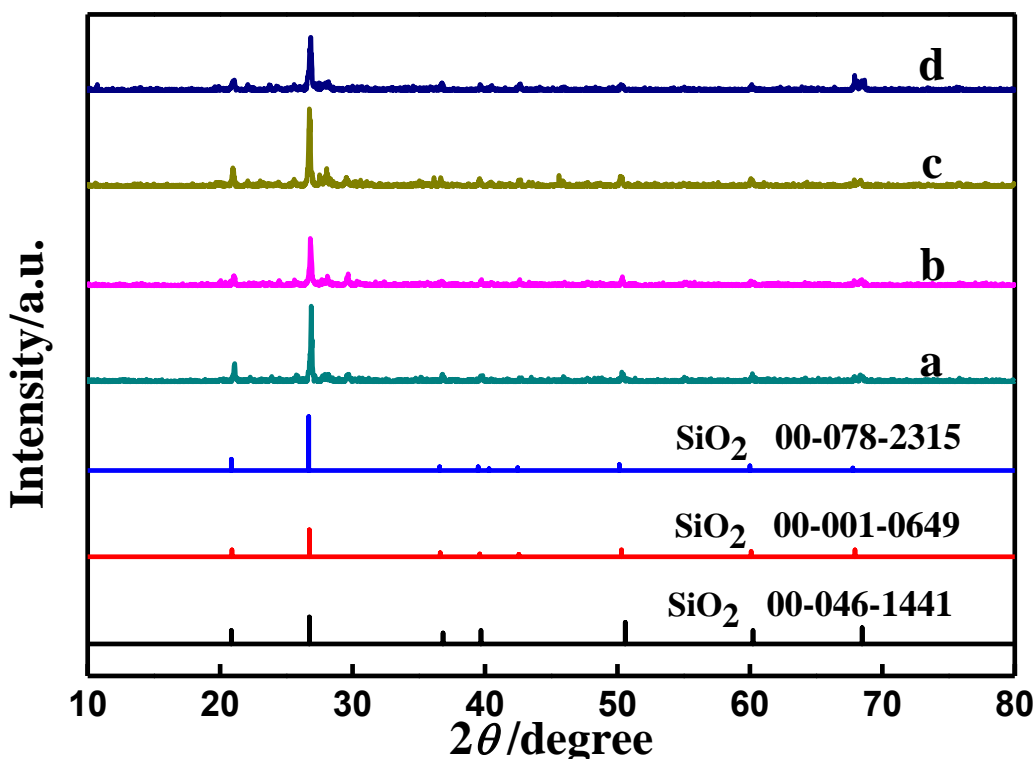## 3. RESULTS AND DISSCUSION

3.1 XRD analysis

Figure 1. XRD patterns of all synthesized materials including some standard XRD patterns of SiO_2. Patterns a, b, c and d were for material a, b, c and d.

The XRD patterns for all prepared materials including the some typical standard XRD patterns of SiO_2 are plotted in Fig.1. In all patterns, a sharp diffraction peak at about 26.8° was seen clearly, which indicated that the main component of all prepared materials was SiO_2 basing on a careful comparison with the standard XRD patterns of SiO_2. Also, the intensities of the diffraction peaks changed correspondingly with the calcination temperature, and the highest diffraction peak of XRD pattern was displayed by material c. Generally, the higher diffraction peak corresponded to a better crystallinity of a material [19]. And the higher crystallinity of an anode material was demonstrated to be beneficial to the lithium ions transferring in an anode material [19]. Thus, material c was expected to deliver a better electrochemical performance owing to its higher crystallinity compared to other materials.
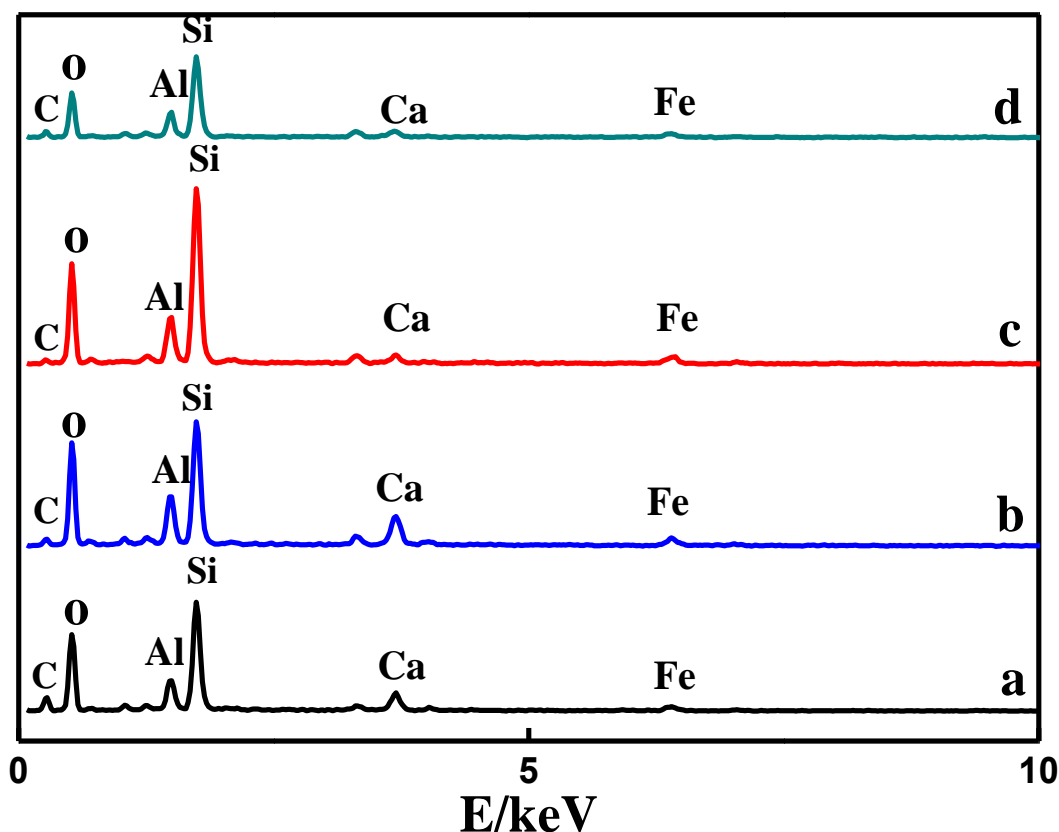
Figure 2. EDS patterns for the obtained materials. Curves a, b, c and d corresponded to material a, b, c and d.

The results of EDS analysis are given in Fig.2 desiring to confirm the element composition of the synthesized materials. The peaks assigned to the elements of C, Al, O, Si, Ca and Fe were clearly displayed in all prepared materials, which, to a great extent, indicated that all the produced materials were a mixture rather than a pure substance though only the diffraction peak corresponding to SiO_2 was displayed in the XRD patterns (Fig.1). The results of the atomic content analysis revealed that C, O and Si were the main three elements in all prepared materials. The atomic contents of C, O and Si were 32.2%, 52.9% and 8.6% for material a, 17.6%, 62.3% and 10.1% for material b, 13.6%, 62.5% and 16.3% for material c, 29.8%, 51.3% and 11.1% for material d, respectively. Thus, for material a, b and c, the atomic content of carbon C decreased with increasing the calcination temperature, which should be due to the combustion of some organic matters in the soils. Evidently, the Si atomic content of material c was the largest one among all prepared materials which indicated that the largest amount of SiO_2 was contained in material c. Also, in the case of material c, the O atomic content should be close to 32% if all the O elements existed in the form of SiO_2, therefore, it was reasonable to believe that besides SiO_2, some metal oxides like Al_2O_3 or Fe_2O_3 were contained in material c. The presence of carbon in material c also demonstrated that material c, instead of a pure substance, was a mixture which contained C, metal oxides and SiO_2.
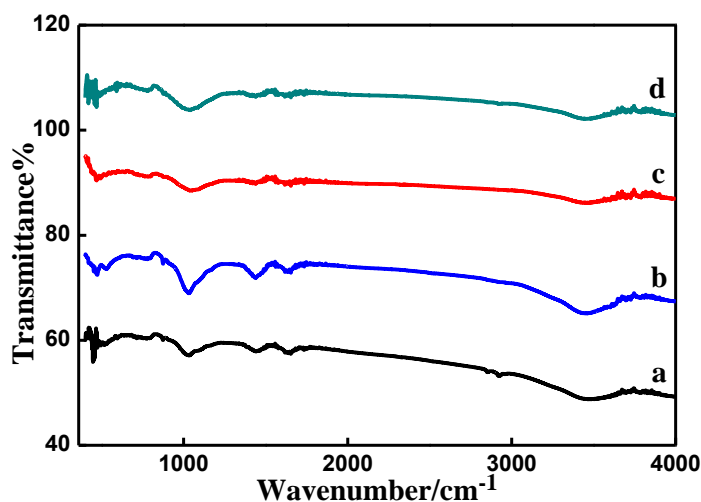
Figure 3. FTIR spectra for all produced materials. Curves a, b, c and d were for material a, b, c and d.

FTIR spectra of all prepared materials were measured and displayed in Fig.3. Clearly, similar shapes of FTIR spectra were presented by all prepared materials which suggested that similar functional groups were contained in the prepared materials. The bands centered at around 1622 cm^{-1} and 3362 cm^{-1} corresponded to the presence of the C-O (from the adsorbed CO_2) and -OH (from the adsorbed H_2O) groups, respectively, basing on the previous work [20]. The bands at 1300-1000, 850-780, and 510-400 cm^{-1} should be attributed to the main absorption modes of SiO_2 [21]. Therefore, the results of FTIR spectra further demonstrated that the main component of all the resultant materials was SiO_2, agreeing well with the results of EDS analysis (Fig.2) and XRD patterns (Fig.1).

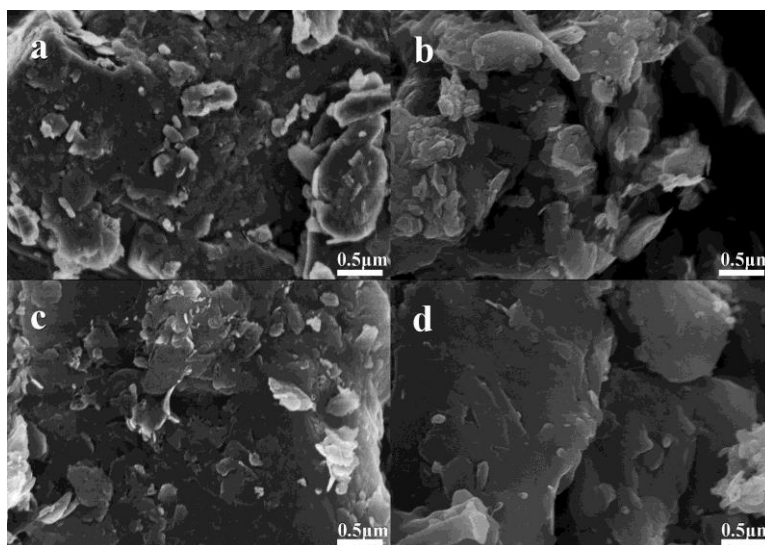*3.2 Morphology characterization*

Figure 4. SEM images for all synthesized materials. Image a, b, c and d corresponded to material a, b, c and d.

Fig.4 illustrates the SEM images of all the prepared materials. For material a, irregular blocky-shaped particles were seen clearly. In the case of material b, some flaky particles were observed. Interestingly, for material c, more amounts of flaky particles were produced. And it seemed that those produced flaky particles were closely packed together in the case of material d. Generally, the larger contacting area of between the electrode material and the electrolyte was favorable to the electrochemical performance improvement due to the significantly reduced over potential according to the Tafel equation [22]. Hence, material c probably could show a better electrochemical behavior when compared to other materials due to the presence of large amounts of flaky particles. Summarily, the results of SEM images strongly indicated that the calcination temperature was a key factor which could affect the morphologies of the resultant materials. Of course, the differed morphologies of electrode materials would lead to a varied electrochemical performance.
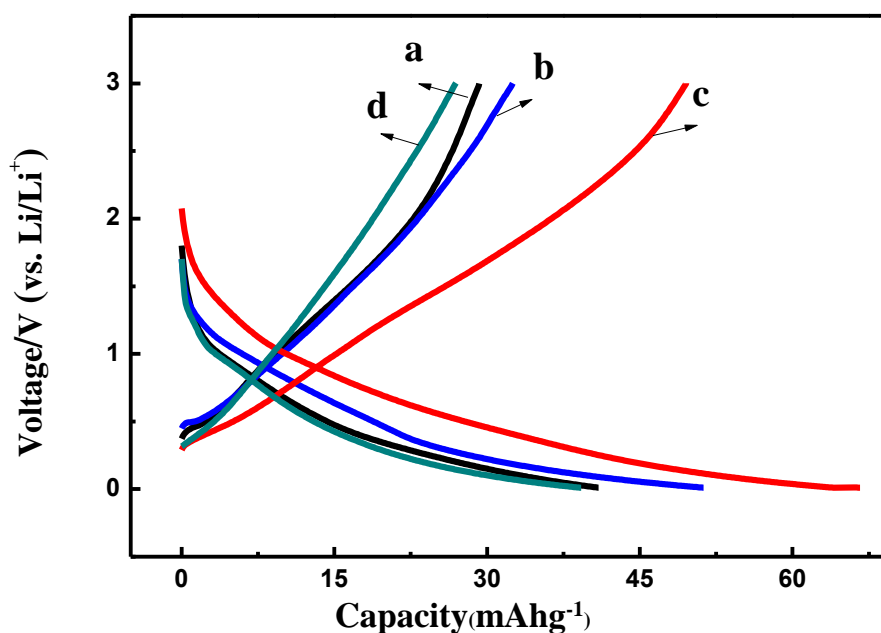
3.3 Electrochemical properties

Figure 5. The initial charge-discharge profiles for all prepared materials which were measured at 100 mA g^{-1}. Line a, b, c and d corresponded to electrode a, b, c and d.

The initial charge-discharge profiles for all prepared electrodes at a current density of 100 mA g^{-1} are presented in Fig.5, in which the potential range was from 0.01 V to 3 V. Apparently, the shape of the charge-discharge curves in Fig.5 was very similar to that of carbon-composited SiO$_2$ electrode [23, 24]. Therefore, the sloped discharge voltage line appearing in 1.00-0.10V should be attributed to the reduction of Si^{4+} and the formation Li-Si-O. And the tilted charge voltage line appearing in 0.10-1.90V should be due to the oxidation reaction of anode material which was commonly accompanied by both the delithiation process and the formation of SiO$_2$. The initial discharge capacities were approximately evaluated to be 41, 51, 67 and 38 mAh g^{-1} for material a, b, c and d at the current

density of 100 mA g^{-1}, respectively. It was really admitted that the initial discharge capacity delivered in this work was rather lower when compared to the currently reported SiO$_2$-based anode material. For example, in 2016, Choy's group [25] prepared SiO$_2$ anode material using tetraethylorthosilicate (TEOS) as the starting material through a chemical method, and found that the initial discharge capacity value of the prepared SiO$_2$ was close to 952 mAh g^{-1} at the current density of 30 mA g^{-1}. In 2017, carbon conformal coating mesoporous hollow SiO$_2$ nanospheres (MHSiO$_2$@C) was developed by Gao's group [26], which showed a high reversible capacity of 440.7 mA h g^{-1} at a current density of 500 mA g^{-1}. Evidently, the complicated preparation processes were involved in above two works which was not advantageous to the large scale production of anode materials. In other words, the simple preparation process and lower preparation cost as well as the acceptable electrochemical performance were the main three factors for a successful commercialization of a newly developed anode material. Although the discharge capacity of the calcined soil was lower when compared to the published SiO$_2$-based composite anode materials, the work described here was very meaningful to the development of anode material, thanks to its rather lower preparation cost and simple preparation process as well as the abundant resources.
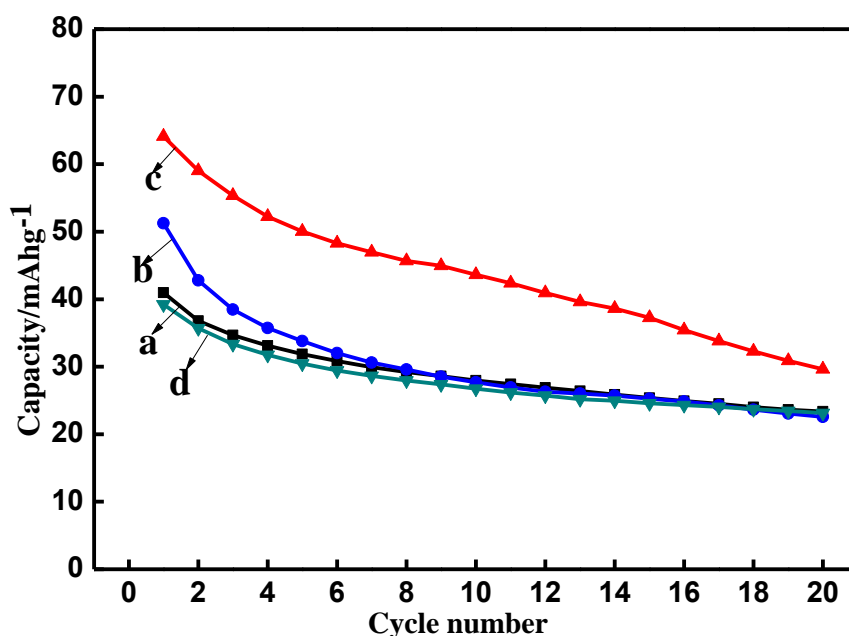

Figure 6. The cycling performances of all prepared electrodes which were plotted at a current density of 100 mA g^{-1}. Curves a, b, c and d were for electrode a, b, c and d.

The cycling stability of all prepared materials was also studied and the results are given in Fig. 6. Apparently, for all synthesized materials, the discharge capacity decreased evidently with increasing the cycling number. The discharge capacities of the first cycle and the 20th cycle for material a, b, c and d was about 41 and 22, 51 and 22, 64 and 30, 39 mAh g^{-1} and 22 mAh g^{-1}, respectively. And in the whole testing period, the largest discharge capacity was delivered by material c, which indicated that material c had the best electrochemical cycling stability among all prepared materials. The relatively

higher crystallinity (Fig.1) and the special flaky morphology (Fig.4) of material c, relative to other materials, should be responsible for its better electrochemical performance.
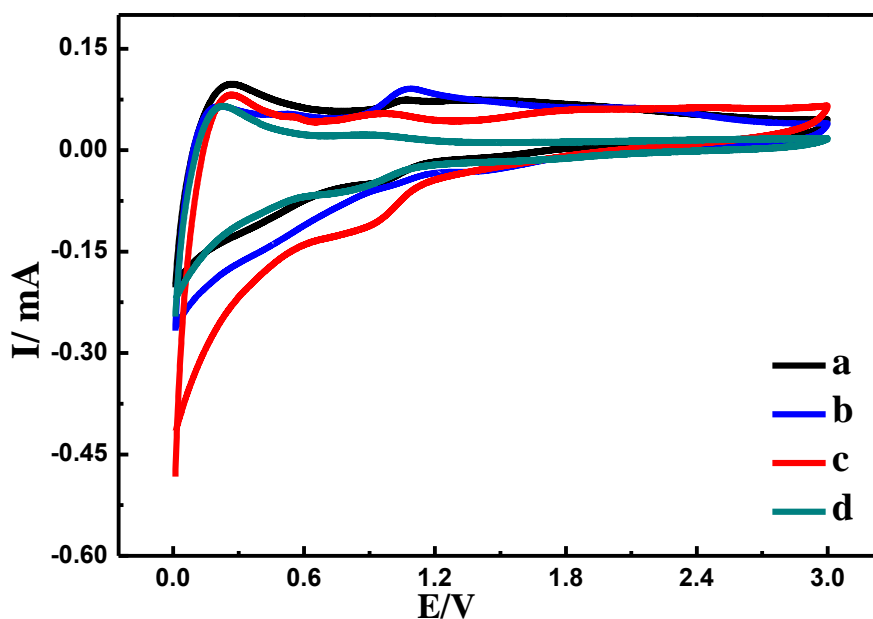

Figure 7. Cyclic voltammetry curves for all the electrodes. Curve a, b, c and d corresponded to material a, b, c and d. The scan rate was 1 mV s^{-1}.

Cyclic voltammetry (CV) curves of the prepared materials were also measured and given in Fig. 7. The presence of redox peaks of CV strongly indicated that the extraction/insertion process of Li ions in the resultant materials could proceed very well. According to the previous work of CV curves for an electrode material [27], the oxidation peak was generally originated from the delithiation process, and the reduction peak was resulted from a lithiation process. Thus, the huge redox peaks centered at about 0 V should be from the reversible alloy-dealloy reaction of silicon with Li ions [24], and the peaks appearing in the potential range of 0.85V-1.35 V should be stemmed from the lithiation/delithiation process of SiO_2. For material a, except for the huge redox peak appearing at 0V, a small oxidation peak and a reduction peak were positioned at about 1.08V and 0.98V, respectively, showing a peak potential separation of about 100 mV ($\Delta E_p = E_{pa} - E_{pc}$). While for material b, only an oxidation peak was seen at about 1.08V, and no evident reduction peak was found in the potential range of 0.85V-1.35V. Although a pair of redox peaks was displayed by material d in the potential range of 0.8V-1.0V, the peak area of CV curve for material d was the smallest one among all prepared samples. Apparently, the CV curve with the largest peak area was displayed by material c, which indicated that the largest amounts of Li ions were transferred in material c, leading to the largest discharge capacity among all prepared materials. Also, the potential separation of the redox peaks of CV curves for material c was about 0.04V ($\Delta E_p = E_{pa} - E_{pc} = 0.95V - 0.91V$), a smaller value. Commonly, the smaller potential separation value corresponded to a better reversibility of an electrode reaction

basing on our previous work [28]. Therefore, material c delivered the best reversibility among all the synthesized materials, being consistent with the results of cycling performance testing (Fig.6).
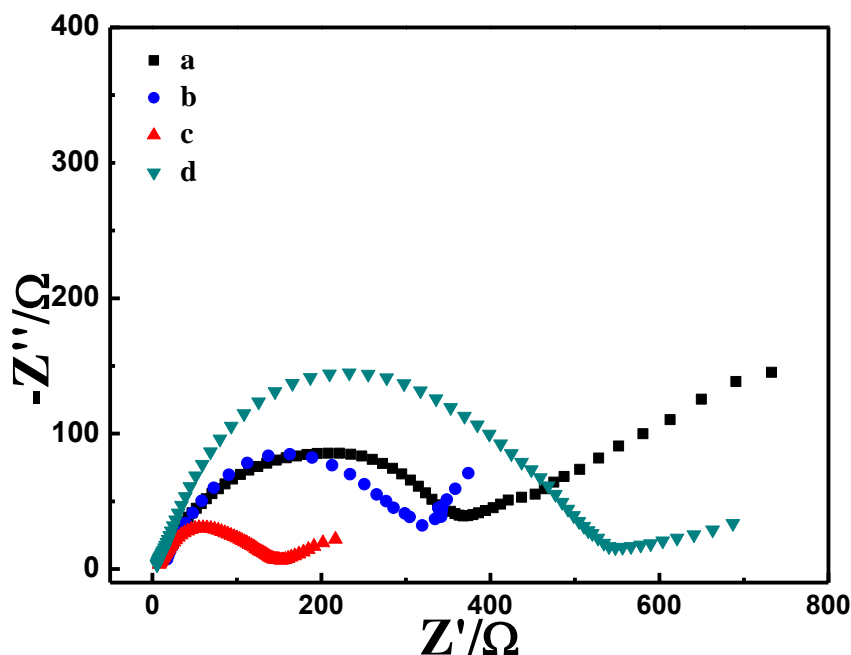

Figure 8. Nyquist plots of all the half-cells assembled by the prepared materials. Curve a, b, c and d corresponded to material a, b, c and d.

Recently, electrochemical impedance spectroscopy (EIS) has become a conventional method for evaluating the electrochemical behavior of a lithium ion half-cell. Nyquist plot, one kind of curves in EIS, mainly due to its simplicity and intuitiveness, has been widely employed as a typical kind of curve from which the electrochemical performances of the electrode materials can be compared directly. The Nyquist plots of all prepared materials were recorded and given in Fig.8. Apparently, the Nyquist plots shown in Fig. 8, for all the electrodes, mainly contained a semicircle in the higher frequency region and a tilted line in the relatively lower frequency region. The shape of Nyqusit plot illustrated in Fig.8 was very near to that of the previously published Nyquist plot regarding a lithium ion half battery. According to our previous work [29], the intercept at the Z' axis was from the whole ohmic resistance (R_Ω), and the presence of the semicircle was generally from a parallel circuit consisting of a resistor unit and a capacitive element. Approximately, the value of the charge transfer resistance (R_{ct}) was equivalent to the diameter value of the semicircle appearing in the Nyquist plot. The presence of the sloped line in the lower frequency region strongly indicated the existence of Warburg impedance, further indicating the presence of the lithium-ion diffusion in an electrode material [29]. Amongst all above parameters, the parameter of R_{ct} is an important parameter through which the kinetics of lithium ion-involved electrode reactions can be compared directly [29]. Namely, the smaller value of R_{ct} represented faster lithium insertion/extraction kinetics. The values of R_{ct} were about 340 Ω, 320 Ω, 137 Ω and 540 Ω, respectively, for electrode a, b, c and d. Therefore, the smallest value of R_{ct} was delivered by electrode c which implied that material c had the fastest lithium

extraction/insertion kinetics among all the resultant materials. This result just explicated the fact that material c displayed the best electrochemical behavior among all the prepared materials.
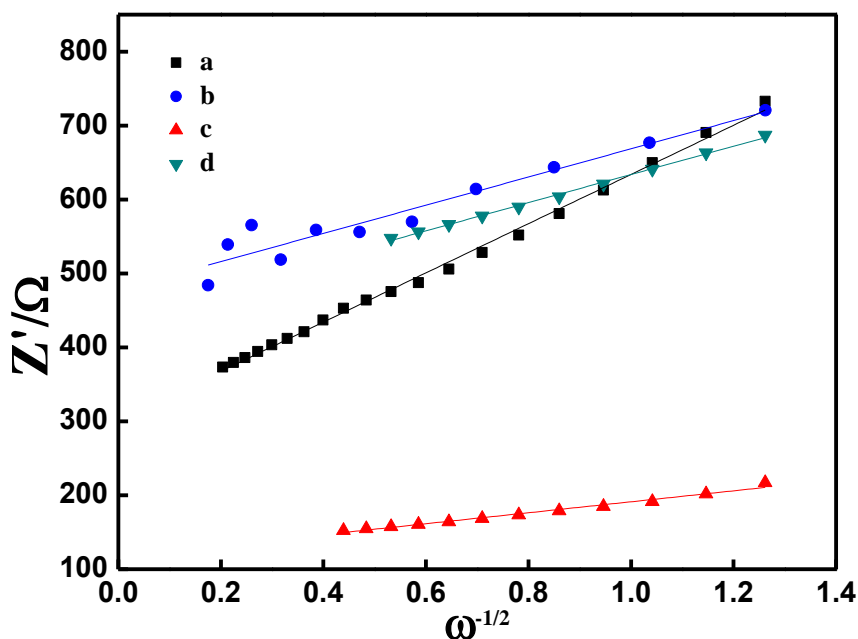

Figure 9. The curves describing the relationship of Z' and the reciprocal of square root of $\omega^{-1/2}$. Curve a, b c and d were for material a, b, c and d.

Except for above parameters, the Li-ion diffusion coefficient, D_{Li}, is also an important parameter from which the diffusion rate of a lithium ion in an electrode material can be estimated roughly. As reported, the value of D_{Li} could be calculated using the following equation [30].

$$D_{Li} = \frac{(RT)^2}{2(An^2F^2C_{Li}\sigma)^2} \qquad (1)$$

Evidently, besides the parameters of R, T and F, the value of D_{Li} was closely related to the parameter of A (surface area of the working electrode), n (the number of electrons transferred in an electrochemical reaction) and C_{Li} (the concentration of lithium ion in a solid anode material). In above equation, σ was called as Warburg factor which can be deduced from the following equation [31].

$$Z_{re} = R_s + R_{ct} + \sigma\,\omega^{-1/2} \qquad (2)$$

In above equation, Z_{re}, R_s and R_{ct} corresponded to Z', the total resistance and the charge transfer resistance, respectively. And ω referred to the angular frequency employed in the low frequency region. The lines of between Z' and $\omega^{-1/2}$ for the resultant four materials are plotted in Fig. 9. As a result, the values of σ can be evaluated directly from these lines. Unfortunately, the exact values of both n and C_{Li} were unknown since the calcined soil was a novel substance which has never been investigated as LIBs anode materials. Thus, the size order of D_{Li} can only be compared approximately when assuming that the values of C_{Li} and n were identical in each material. Obviously, a larger value

of D_{Li} should correspond to a smaller value of σ. Thus, the value of D_{Li} for material c was the largest one among all the material due to its smallest value of σ. It effectively indicated that the diffusion rate of lithium ions in material c was the largest one among all the prepared materials, which just interpreted the result that material c delivered the best electrochemical performance among all the materials.

4. CONCLUSION

For the first time, an interesting finding, that the calcined soils can be used as anode materials for LIBs, is reported in this communication, though the discharge capacities of the calcined soils were lower when compared to the currently published anode materials. The results of XRD indicated that SiO_2 was the main component of the prepared materials. SEM images revealed that the calcination temperature has remarkably influenced the morphologies of the resultant materials, and flaky particles were seen when calcination temperature was 600 °C. The results of electrochemical measurements indicated that 600 °C-calcined soil delivered the best electrochemical performance among all the synthesized materials. This work, at least, has evidenced the possibility of using calcined soil as anode materials for LIBs, which was very helpful to the development of the commercial LIBs, because of the rather lower preparation cost and rather simple preparation process as well as the abundant resources of the starting materials.

References

1. M. Gockeln, S. Pokhrel , F. Meierhofer, J. Glenneberg, M. Schowalter ,A. Rosenauer, U. Fritsching, M. Busse, L. Mädler and R. Kun, *J. Power Sources* ,374 (2018) 97.
2. X. Lu, L. Gu, Y.-S. Hu, H.-C. Chiu, H. Li, G. P. Demopoulos and L. Chen, *J. Am. Chem. Soc.*, 137 (2015)1581.
3. P.P. Wang, Y.X. Zhang, X.Y. Fan, J.X. Zhong and K. Huang, *J. Power Sources*, 379 (2018) 20.
4. H. Tian , X. Tan, F. Xin , C. Wang and W. Han, *Nano. Energy*, 11 (2015) 490.
5. S. Fang, D. Jackson, M. L. Dreibelbis , T. F. Kuech and R. J. Hamers, *J. Power Sources,* 373 (2018) 184.
6. Y. Cen, Q. Qin, R. D. Sisson and J. Liang, *Electrochim. Acta* , 251 (2017) 690
7. X. Li, N. Fu, J. Zou, X. Zeng, Y. Chen, L. Zhou, W. Lu and H. Huang, *Electrochim. Acta,* 225 (2017) 137.
8. L. Zhang, G. Xia, Z. Guo, D. Sun, X. Li and X. Yu, *J. Power Sources,* 324 (2016) 294.
9. K. Ding, P. Wang, J. Zhao, Y. Li, Y. Chen, Y. Zhang, B. Wei, Y. Sun and J. Pan, *Int. J. Hydrogen. Energy*, 42 (2017) 9766.
10. L. Liu, H. Zhang, S. Liu, H. Yao, H. Hou and S. Chen, *Electrochim. Acta* 219 (2016) 356.
11. Y. Wang, J. Roller and R. Maric, *J. Power Sources,* 378 (2018) 511.

12. Q. Tiana, L. Li, J. Chen, L. Yang and S.-i. Hirano, *J. Power Sources*, 376 (2018) 1.
13. Z. Li, X.-Y. Yu and U. Paik, *J. Power Sources,* 310 (2016) 41.
14. Y. Feng, H. Zhang, W. Li, L. Fang and Y. Wang, *J. Power Sources,* 301 (2016) 78.
15. S. Cho, H. Y. Jang, I. Jung, L. Liu and S. Park, *J. Power Sources*, 362 (2017) 270.
16. I. Meschini, F. Nobili, M. Mancini, R. Marassi, R. Tossici, A. Savoini, M. L. Focarete and F. Croce, *J. Power Sources*, 226 (2013) 241.
17. K. Ding, J. Zhao, J. Zhou, Y. Zhao, Y. Chen1, Y. Zhang, B. Wei, L. Wang and X. He, *Int. J. Electrochem. Sci.*, 11 (2016) 446.
18. K. Ding, J. Zhao, J. Zhou, Y. Zhao, Y. Chen, L. Liu, L. Wang, X. He and Z. Guo, *Mater. Chem. Phys.*, 177 (2016) 31.
19. K. Ding, H. Gu, C. Zheng, L. Liu, L. Liu, X. Yan and Z. Guo, *Electrochim. Acta*, 146 (2014) 585.
20. K. Ding, J. Zhao, Y. Sun, Y. Chen, B. Wei, Y. Zhang and J. Pan, *Ceram. Int.*, 42 (2016) 19187.
21. K. Kim, H. Choi and J.-H. Kim, *Appl. Surf. Sci*, 416 (2017) 527.
22. K. Ding, Y. Zhao, M. Zhao, Y. Li, J. Zhao, Y. Chen and Q. Wang, *Int. J. Electrochem. Sci.,* 10 (2015) 7917.
23. Y. Yao, J. Zhang, L. Xue, T. Huang and A. Yu, *J. Power Sources*, 196 (2011) 10240.
24. B. Guo, J. Shu, Z. Wang, H. Yang, L. Shi, Y. Liu and L. Chen, *Electrochem. Commun.,* 10 (2008) 1876.
25. D.W. Choi and K.-L. Choy, *Electrochim. Acta*, 218 (2016) 47.
26. W. An, J. Fu, J. Su, L. Wang, X. Peng, K. Wu, Q. Chen,Y. Bi, B. Gao and X. Zhang, *J. Power Sources*, 345 (2017) 227.
27. K. Ding, Y. Zhao, L. Liu, Y. Li, L. Liu, L. Wang, X. He and Z. Guo, *Electrochim. Acta*, 176 (2015) 240.
28. K. Ding, T. Okajima and T. Ohsaka, *Electrochemistry*, 75 (2007) 35.
29. K. Ding, B. Wei, Y. Zhang, C. Li, X. Shi and J. Pan, *Int. J. Electrochem. Sci.*, 12 (2017) 8381.
30. A.Y. Shenouda and H.K. Liu, *J. Power Sources*, 185 (2008) 1386.
31. T.-F. Yi, H. Liu, Y.-R. Zhu, L.-J. Jiang, Y. Xie and R.-S. Zhu, *J. Power Sources*, 215 (2012) 258.